Paper No.
62—WA-70

Longitudinal Strain Pulse Propagation in Wide Rectangular Bars[1]

Part 2—Experimental Observations and Comparisons With Theory

O. E. JONES[2]
Research Engineer,
Hydrodynamics Laboratory,
California Institute of Technology,
Pasadena, Calif.

A. T. ELLIS
Associate Professor of Applied Mechanics,
California Institute of Technology,
Pasadena, Calif.

The plane-stress theory presented in Part 1 is shown to predict qualitatively the warping of plane sections observed in transient fringe patterns obtained using birefringent coatings and in dynamic photoelastic pictures obtained in other investigations. Measurements using conventional techniques are described in which wide rectangular bars were subjected to a longitudinal step-function pressure loading produced by a shock tube. Comparisons show that the gross features of the experimental records for the head of the pulse are qualitatively predicted by the theory. Both theory and experiment show that short-wavelength, second-mode disturbances arrive very early. Experimentally it is observed that these disturbances are accomplished by thickness-mode activity which cannot be accounted for by the plane-stress theory.

In the companion paper, Part 1, asymptotic expressions were obtained which, for large distances of travel, describe the longitudinal elastic-strain wave propagation in a semi-infinite, plane-stress elastic strip with stress-free lateral edges subject to the conditions that a uniform normal pressure with a step-function time dependence is applied to the end and that the end is laterally constrained.

The purpose of this part of the paper is to determine the usefulness of these expressions by comparing them with experimental observations. Theoretical predictions of the plane-stress theory for the warping of plane sections are compared with transient fringe patterns obtained using birefringent coatings and with dynamic photoelastic pictures obtained by other investigators. An extensive experimental program using conventional strain-measuring techniques is described in which wide rectangular aluminum bars of several thicknesses were subjected to step-function pressure loadings produced by a shock tube. This program was undertaken for the purpose of providing more critical tests of the plane-stress theory and gaining further insight into the physical problem. Comparisons are made between the results of these experiments and the theoretical predictions.

Warping of Plane Sections

Observed Fringe Patterns. Birefringent coatings[3] were considered as an experimental means of studying wave-propagation phenomena in metals and preliminary experiments were undertaken to determine whether it is technically possible to photograph the resulting fringe patterns. Using a Kerr cell motion-picture camera developed by one of the authors,[5] the ultrahigh-speed motion pictures shown in Fig. 1 were obtained for transient fringe patterns resulting from the hammer impact of one end of a rectangular aluminum bar having a birefringent coating.[6] The time between consecutive frames is 10 microsec and the exposure time is approximately 0.05 microsec. Although further experiments are required to determine whether the fringe patterns truly represent the surface strains, several interesting observations can be made from Fig. 1. The uniformly bright field of frames 1, 2, and 3 indicates that the wave has not yet arrived. The fringe pattern at the top of frame 4 indicates that the hammer hit on one corner. In frame 5 the symmetric shape of the fringe pattern suggests that bending modes are no longer present at the head of the pulse. Between frames 4 and 5 the fringe pattern appears to travel with the metal wave velocity of approximately 2×10^5 ips, which is reassuring. The pronounced concave curvature of the leading fringes with respect to the direction of wave propagation in frame 5 indicates that plane sections of the bar are warping for relatively long-wavelength waves. If there was no warpage, the fringes would have no curvature. The remaining frames, beginning with frame 6, show very complex and confused fringe patterns of unknown origin. They are probably due to short-wavelength, high-frequency waves traveling in the bar and to associated coating-thickness effects. Because dispersion is not so important near the point of impact, high-frequency waves are expected to be strongly present very early in the wave train.

Since dynamic photoelasticity can give some qualitative insight into elastic-wave propagation, it is interesting to note that similar fringe curvatures are present to some degree in all the full-field dynamic photoelastic fringe patterns which have been obtained for the longitudinal impact of rectangular bars. Concave curvatures of the leading fringes with respect to the direction of wave propagation are observed in the pictures of Sutton [3] and Feder, et al. [4]. In the pictures of Durelli, et al. [5, 6], the curvature continuously changes from concave to convex as the fringe order increases to its maximum value.

[1] The results presented here were obtained in the course of research sponsored in part by U. S. Naval Ordnance Test Station Contract N123(60530)24917A and National Science Foundation Grant G-2586.

[2] Presently Staff Member, Sandia Corporation, Albuquerque, N. Mex.

[3] Static applications of birefringent coatings have been reviewed recently by Hetényi [1].[4]

Contributed by the Applied Mechanics Division for presentation at the Winter Annual Meeting, New York, N. Y., November 25–30, 1962, of The American Society of Mechanical Engineers.

Discussion of this paper should be addressed to the Editorial Department, ASME, United Engineering Center, 345 East 47th Street, New York 17, N. Y., and will be accepted until one month after final publication of the paper itself in the Journal of Applied Mechanics. Manuscript received by ASME Applied Mechanics Division, June 12, 1961. Paper No. 62—WA-70.

[4] Numbers in brackets designate References at end of paper.

[5] Ellis [2] has described this camera in connection with other applications.

[6] The bar dimensions are 0.250 in. × 0.978 in. × 10.75 in. A 0.120-in-thick layer of PhotoStress plastic served as the birefringent coating. Although the coating should be extremely thin, it was necessary to use a relatively thick coating in order to obtain photographically significant fringe orders.

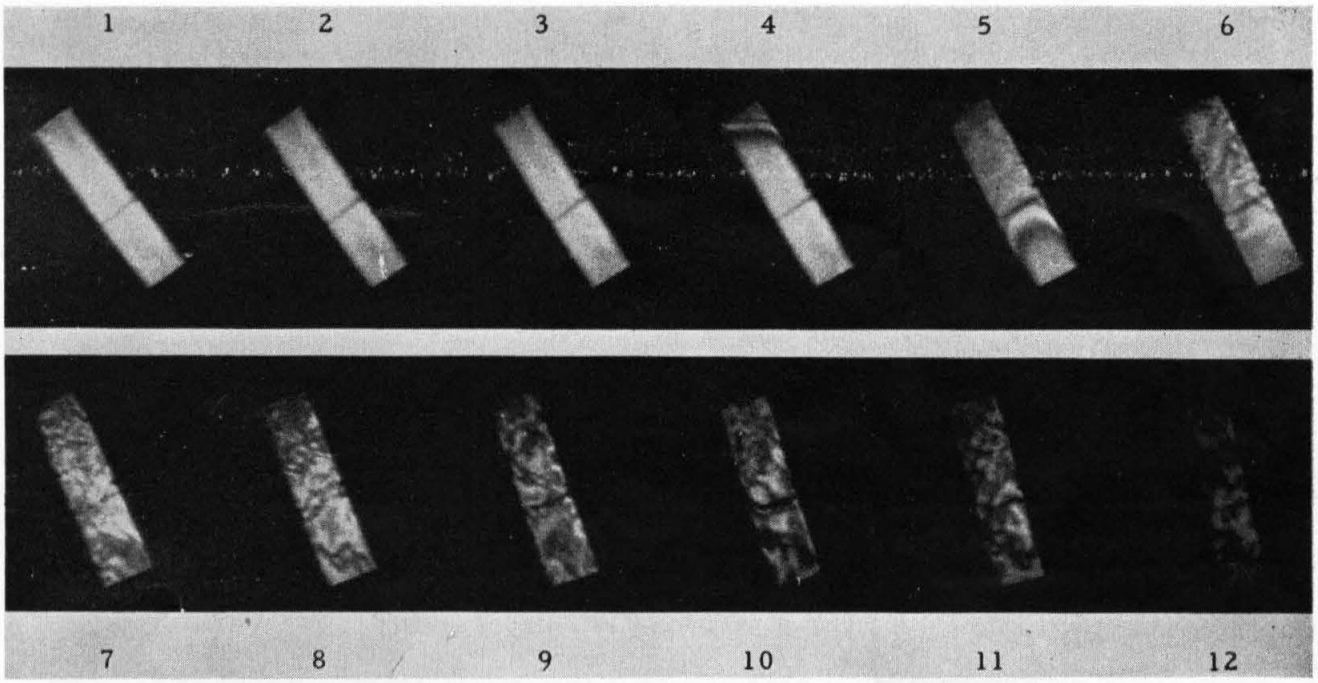

Fig. 1 Ultra-highspeed motion pictures of transient fringe patterns resulting from impacting an aluminum bar having a birefringent coating. Field of view begins $^{3}/_{4}$ in. from impacted end and extends 3 in. along bar; stationary dark line is a shadow

Comparison of Observed and Predicted Fringe Patterns. The fringe patterns in Fig. 1 were obtained for a longitudinal impact type of input whereas the expressions developed in Part 1 are for a pressure-shock type of input. For large distances from the source it is reasonable to expect that the solutions for longitudinal impact and pressure-shock problems would be essentially equivalent (cf. Miklowitz [7]). Although the fringe curvatures noted in Fig. 1 were observed relatively near the impacted end, it is expected that similar, but less pronounced, curvatures of the leading fringes would be observed at stations more distant from the end. This is the case in the pictures obtained by Durelli, et al [5, 6]. On the basis of these arguments, which may not be completely valid, the observed fringe curvatures at the head of the pulse will be compared qualitatively with the theoretically predicted curvatures.

For purposes of qualitative comparison it will be assumed that the isochromatic fringe order N observed at a point is proportional to the absolute value of the difference of the principal strains e_1 and e_2 at the point. In terms of the strain components e_{xx}, e_{yy}, and e_{xy}, the absolute value of the principal strain difference is

$$|e_1 - e_2| = + [(e_{xx} - e_{yy})^2 + (e_{xy})^2]^{1/2}$$

Considering only first-mode contributions to the head of the pulse, the expressions for e_{xx}, e_{yy}, and e_{xy} are given by (38), (39), and (40), respectively, of Part 1. Some typical calculated first-mode contours of constant principal-strain difference are shown in Fig. 2. The solid lines identify contours obtained using only the first two terms in each of expressions (38) and (39) of Part 1 for e_{xx} and e_{yy}. For comparison several contours, indicated by dashed lines, are shown for which all three terms are included. In general, the additional terms serve to shift a particular contour and increase its curvature; otherwise, the general contour pattern is the same in both cases.

Fig. 2 will be taken as qualitatively representing the predicted first-mode fringe pattern at the head of the pulse. The leading fringes have concave curvatures with respect to the direction of wave propagation. As the fringe order increases, the curvature continuously changes from concave to convex. A fringe having essentially no curvature, indicating a uniaxial stress state, marks the transition from concave to convex curvatures. The fringe curvatures then become increasingly convex with the result that the fringes begin to close upon themselves, essentially appearing as ellipses of continuously decreasing size centered about a point. The point is a fringe source and it corresponds to the maximum fringe order at the head of the pulse. Continuing along the strip center line, the fringe order decreases and the closed fringes give way to fringes having convex curvatures with respect to the direction of wave propagation. It can be shown readily that the theory predicts that this general pattern is repeated for the first mode. Thus the fringe source in Fig. 2 is followed by a fringe sink, a second fringe source (of lesser order than the first), a second fringe sink, and so on.

The predicted first-mode fringe pattern in Fig. 2 cannot be compared with the observed fringe pattern in Fig. 1 without first examining the influence of the higher modes. For relatively

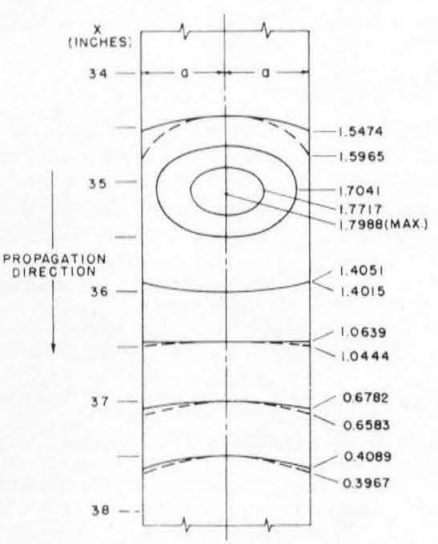

Fig. 2 Predicted first-mode contours of constant principal-strain difference $(E/P_0)|e_1 - e_2|$ at head of pulse. t = 183.9 microsec, c_s = 0.1248 in. per microsec, σ = 0.335, and a = 0.75 in.

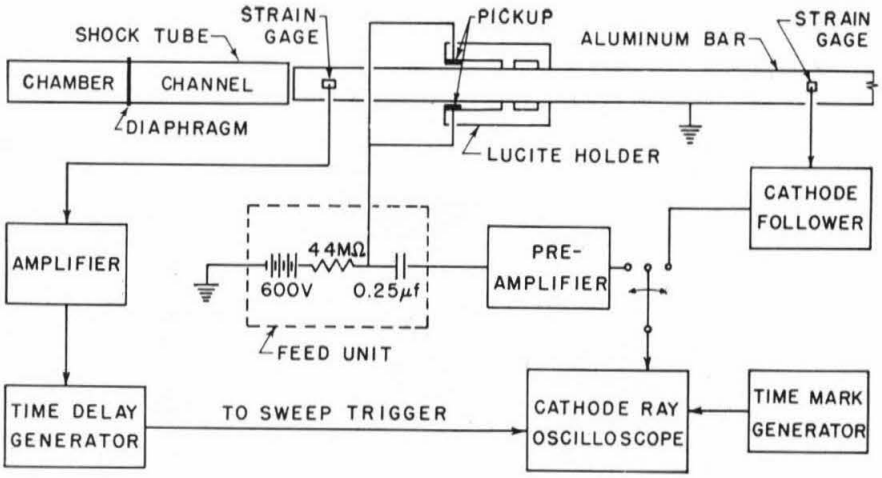

Fig. 3 Schematic apparatus diagram

short distances from the loaded end the initial arrivals of the second-mode disturbances quite closely follow the leading first-mode disturbances (Figs. 5 and 6); consequently, the beginning second-mode disturbances, given by (45), (46), and (47) of Part 1, are expected to influence the leading edge of the pulse. Rough calculations for stations ahead of the fringe source in Fig. 2 indicate that second-mode contributions modify individual contours considerably, but that the general contour pattern of the leading fringes is unchanged. Qualitatively, then, the theory predicts the observed concave curvature of the leading fringe in Fig. 1.

It has been pointed out already that dynamic photoelasticity can give qualitative indications of elastic-wave-propagation phenomena. In the usual viscoelastic photoelastic materials, the high-frequency components of a pulse are generally much more severely attenuated [3] than those of lower frequency. Consequently, it is assumed that dynamic photoelastic fringe patterns obtained for the longitudinal impact of wide rectangular bars primarily reflect the behavior of the first mode and are best compared to the predicted first-mode fringe pattern in Fig. 2.

The predicted concave curvatures of the leading fringes are observed in the dynamic photoelastic pictures of Sutton [3] and Feder, et al [4] for the longitudinal impact of rectangular bars of CR-39. Further comparisons between their pictures and Fig. 2 are not justified because of varying combinations of low fringe orders, poor resolution, and loading problems.

Dynamic fringe patterns obtained by Durelli, et al [5, 6] for longitudinally impacted rectangular bars of Hysol 8705, a low-modulus material, are quite interesting in terms of the predicted first-mode fringe patterns. Using this material, maximum fringe orders of ten are easily attained and the transient fringe patterns can be photographed using relatively conventional techniques. A comparison, for example, of Fig. 69 of [6] with Fig. 2 of the present paper indicates that there is striking qualitative agreement between the observed and predicted first-mode fringe patterns at the head of the pulse. The theory properly predicts the observed concave curvatures of the leading fringes, the observed transition from concave to convex curvatures with increasing fringe order, the observed fringe source for the maximum fringe order, and the subsequently observed succession of increasingly closely spaced fringe sources and sinks.

More Critical Tests of the Theory

In view of the good qualitative agreement between observed and predicted fringe patterns, an experimental program was undertaken for the purpose of providing more critical tests of the theory. The results of this program should be of general interest since very little experimental information is presently available in the literature for the propagation of longitudinal strain pulses in rectangular bars.

Experimental Apparatus. The general experimental arrangement is shown in Fig. 3. Stress is applied to one end of a long rectangular aluminum bar by the reflection of a shock wave in air from the end face. The shock wave is produced in a conventional shock tube by bursting a diaphragm between a high-pressure chamber and a channel originally at atmospheric pressure.

The stress applied to the end of the bar has a component only in the normal direction and is uniform over the entire end face. Since all measurements are made during the time the pressure remains constant, the time dependence of the applied stress may be considered as a step function. This method of loading, then, experimentally provides the step-function pressure loading considered in the mathematical treatment of Part 1; but does not duplicate the other mathematical end condition of lateral constraint. It was pointed out in Part 1 that failure to satisfy the lateral end condition is expected to be relatively unimportant for strains at large distances from the end.

To investigate the influence of bar thickness, strain measurements were made for three rolled 2024 T4 aluminum bars having essentially the same widths but different thicknesses. The respective cross-sectional dimensions of the three bars were 0.064 in. by 1.484 in., 0.126 in. by 1.501 in., and 0.252 in. by 1.501 in. Each of the bars was 130 in. long. With bars of this length it was possible to observe most of the interesting features of the head of the strain pulse for distances of travel up to about 115 in.

In order to evaluate any of the equations developed in Part 1 to predict the nature of the strain pulse, a knowledge of the elastic constants of the three bars is required. The elastic constants were measured for a specimen machined from the 0.252-in-thick bar by using the pulse method described by Hughes, Pondrom and Mims [8]. On the basis of these measurements, the shear-wave velocity c_s and Poisson's ratio σ were taken as 0.1248 in. per microsec and 0.335, respectively, for the three bars.

As shown in Fig. 3, a condenser-microphone arrangement is used to measure changes in the bar width. In order to isolate the pickups from any disturbance transmitted to the lucite holder during the recording of a signal, the pickups are cantilevered with respect to the holder supports. This provides an undisturbed recording time of at least 80 microsec. Square barium-titanate strain gages mounted midway between the bar edges at several stations along one side of the bar are used to measure the sum of the principal strains. Square gages are used to insure against bond cross-sensitivity effects [9].

General Discussion of Experimental Records. The experimental records are shown in Fig. 4 for stations $x = 37.5$ in. and 112.5 in.[7]

[7] Similar sets of records, which are not shown here, were also obtained for stations $x = 18.75$ and 75.0 in.

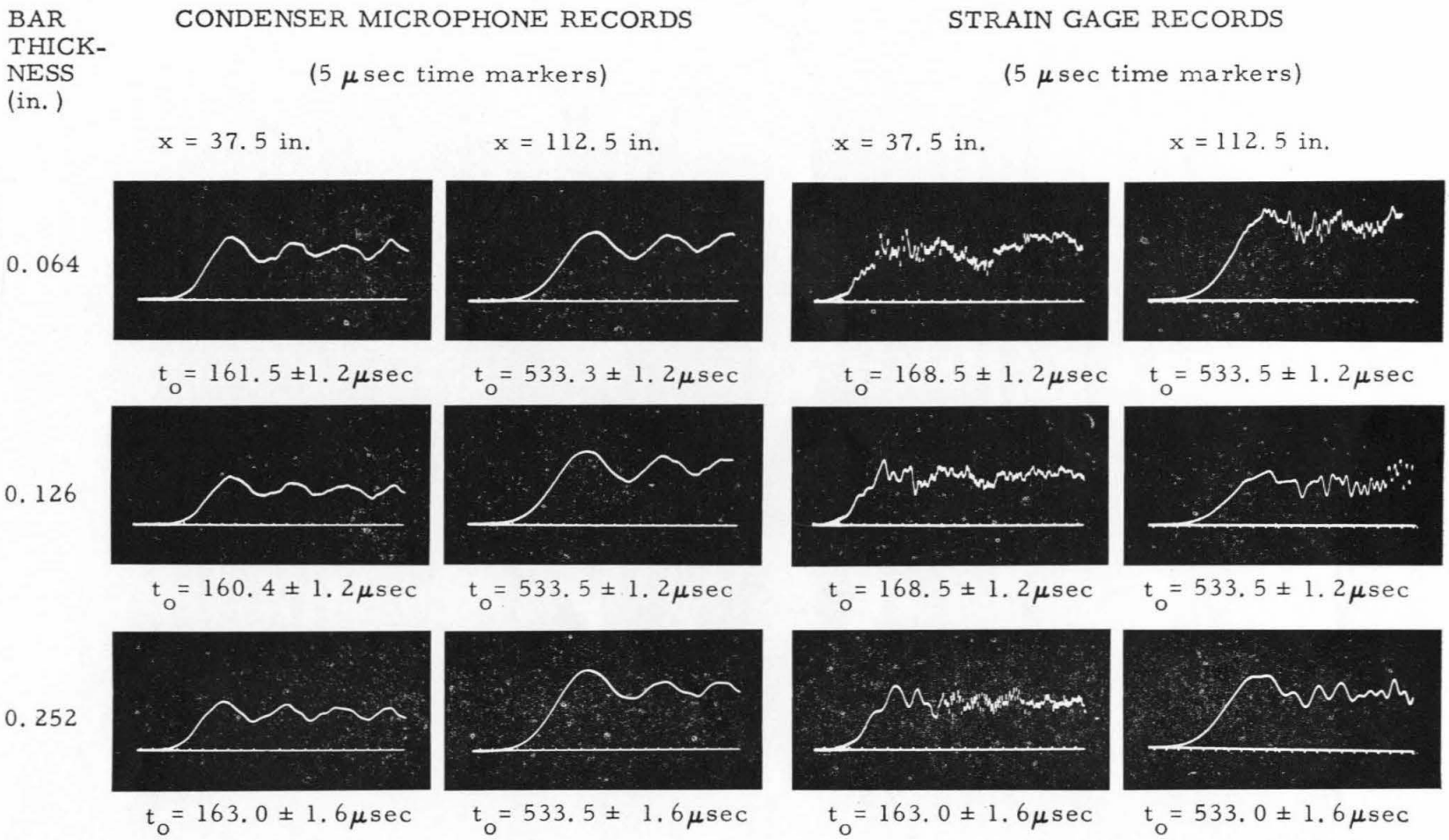

Fig. 4 Experimental records for strain pulse at stations x = 37.5 and 112.5 in. resulting from step-pressure loading of three rectangular aluminum bars of different thicknesses

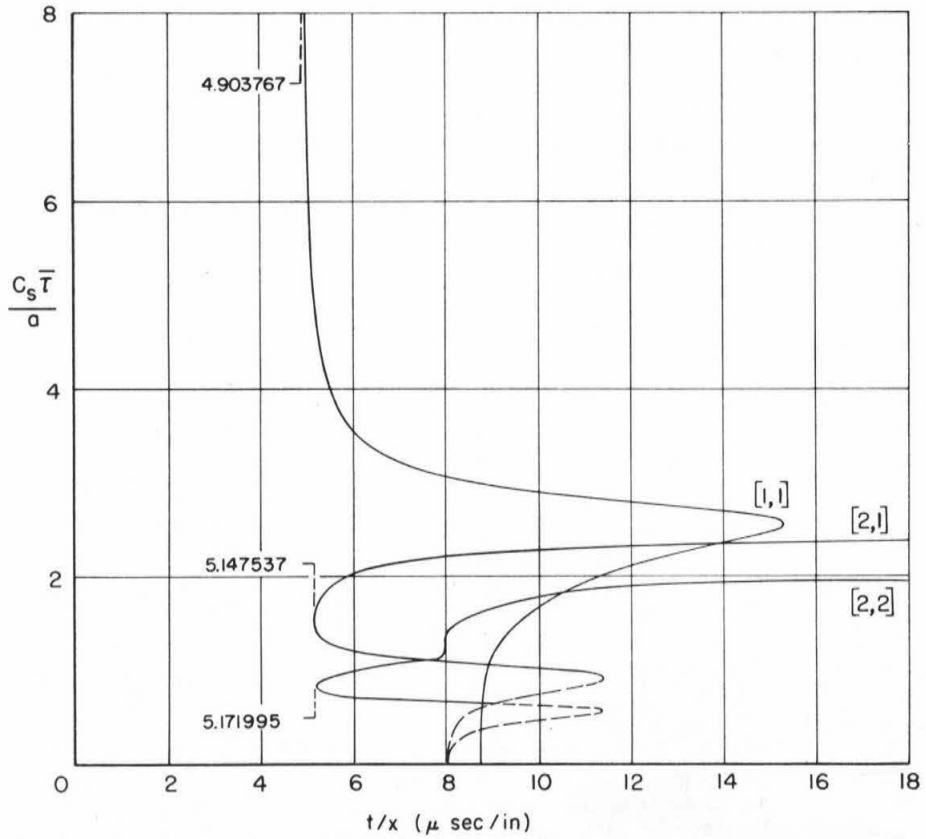

Fig. 5 Dominant periods $(c_s \bar{T})/a$ associated with real [1,1], [2,1], and [2,2] saddle points as functions of time t for a given station x ($\sigma = 0.335$). Dashed portions indicate approximate values.

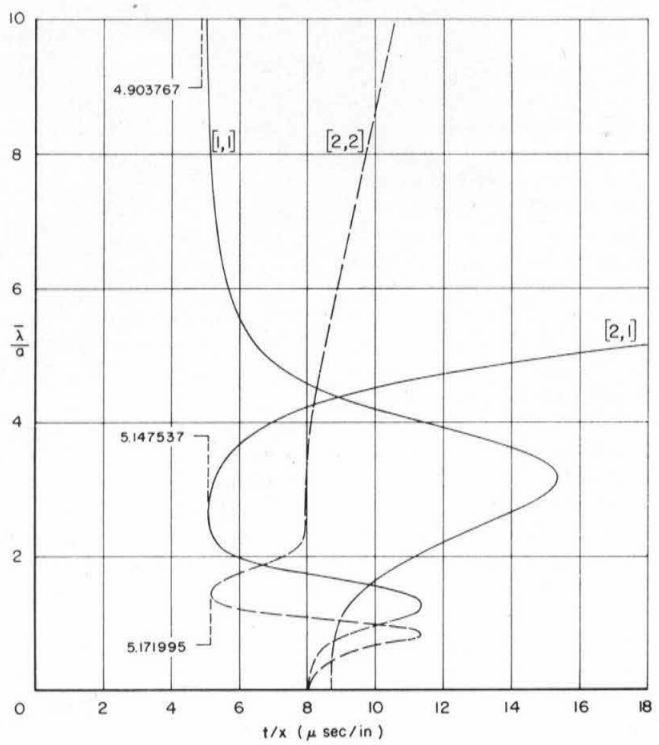

Fig. 6 Dominant wavelengths $\bar{\lambda}/a$ associated with real [1,1], [2,1], and [2,2] saddle points as functions of t for a given station x ($\sigma = 0.335$). Dashed portions indicate approximate values.

For each station, condenser-microphone and barium-titanate strain-gage records are shown for the three bars just described. For a condenser-microphone record, the output is expected to be proportional to the change in bar width; for a strain-gage record, the output is proportional to the sum of the principal strains midway between the edges of one side of the bar. Measuring from the instant of load application, the starting time and estimated limits of error are given for each record by $t = t_0$.

All of the records were found to be highly reproducible with respect to time. For a particular record, only the relative amplitudes of the oscillations are important since no attempt was made to measure absolute magnitudes of either the applied pressure or the resultant strains in the bar. Unfortunately, the relative amplitudes at a given station for a particular bar and detector were not as reproducible as the time variations. Differences ranging up to 8 percent were observed for 0.126 and 0.252-in-thick bars, and up to 15 per cent for the 0.064-in-thick bar. The cause of these differences is not known. However, the extreme flexibility of the 0.064-in-thick bar may be worth noting.

If there was no dispersion, the experimental records would have the simple form of a step function. Clearly, they bear only a rough resemblance to a step. The strain-gage records, in particular, exhibit complicated behavior very shortly after the initial arrival of the pulse. This is in agreement with the arrival time predictions of the approximate ordinary saddle-point, or group-velocity, analysis of the theory. According to this analysis, saddle points corresponding to the real $\alpha_{2,1}$ branch of the second mode for positive β become real very shortly after the first-mode saddle points become real. The analysis also indicates that saddle points associated with the real $\alpha_{2,2}$ branch of the second mode for positive β become real almost immediately after the initial second-mode arrivals. For convenience, these groups of saddle points and their contributions will be labeled [1, 1], [2, 1], and [2, 2], respectively. For $\sigma = 0.335$, Figs. 5 and 6 show, respectively, the dominant period $\bar{\tau}$ and wavelength $\bar{\lambda}$ associated with the real [1, 1], [2, 1], and [2, 2] saddle points as a function of time t for a particular station x. The minimum values of t/x for which the saddle points first become real (corresponding to the formation of third-order saddle points) are given in these figures. For moderate distances of travel x, it is clear from these values that second-mode contributions to the strain pulse should be present at the head of the pulse.

Morse's experimental work (see Part 1, reference [2]) for wide rectangular bars indicates that no propagation takes place in the lowest thickness mode below a cut-off frequency which occurs when $\bar{\lambda}/a = 4$; i.e., when the half-wavelength is equal to the bar width. From Fig. 6 it is observed that both of the initial second-mode arrivals violate this condition; thus it is expected that thickness effects should be observable in the experimental records. Indeed, oscillations associated with the bar thickness are clearly observed in the leading portions of the strain-gage records for station $x = 37.5$ in.

The condenser-microphone records, on the other hand, exhibit relatively much less complicated behavior than the corresponding strain-gage records. In general agreement with these records, it will be shown in the next section that the theory predicts that the initial second-mode contributions to the change in width of the bar are negligible at the head of the pulse.

In the following sections the theoretical predictions of Part 1 for the head of the pulse are compared in detail with the observed experimental behavior. The predictions are based on a Poisson's ratio σ of 0.335, a shear-wave velocity c_s of 0.1248 in. per microsec, and a strip half-width a of 0.75 in.

Comparison of Condenser Microphone Records With Theory. The predicted condenser-microphone response, which is proportional to the transverse displacement v at the edge $y = a$ of the strip, is shown in Figs. 7(a) and (b) for the head of the pulse at stations $x = 37.5$ and 112.5 in., respectively. The first-mode contribution is obtained by integrating (39) of Part 1 across the strip half-width. The second-mode contributions are obtained by integrating (46) of Part 1 across the strip half-width and evaluating the resulting expression separately for each of the two initial second-mode arrivals.

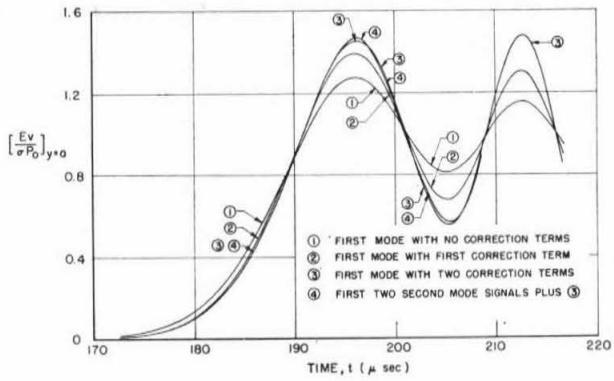

(a) $x = 37.5$ in.

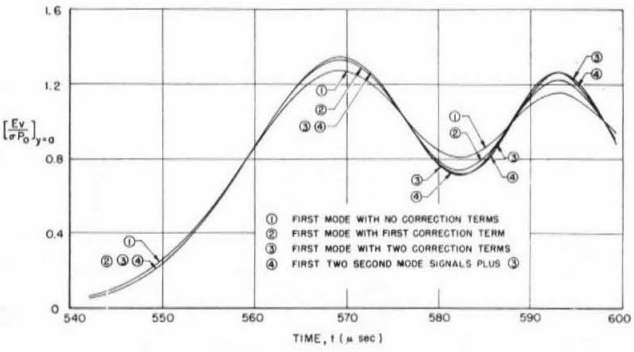

(b) $x = 112.5$ in.

Fig. 7 Predicted displacement $(Ev)/(\sigma P_0)$ at strip edge $y = a$ for head of pulse. $c_s = 0.1248$ in. per microsec, $\sigma = 0.335$, $a = 0.75$ in.

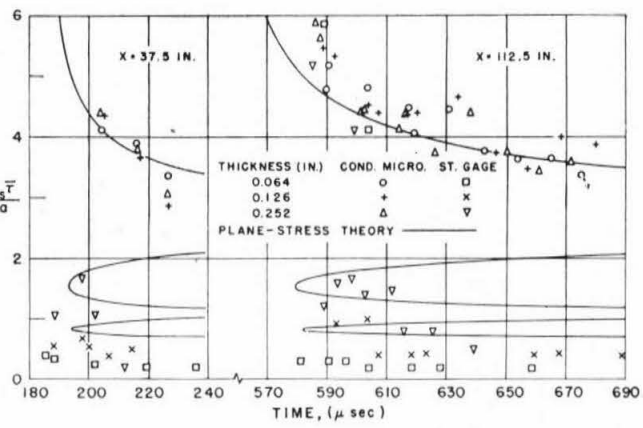

Fig. 8 Comparison of measured values for the dominant periods $(c_s \bar{\tau})/a$ of observed oscillations with predictions of ordinary saddle-point approximation

It is clear that the first-mode correction terms, which describe the nonuniform strain distribution across the strip for the first mode, serve to magnify the changes in the strip width. The magnitude of these correction terms decreases with the distance of travel. The second-mode contributions, as shown in Figs. 7(a) and (b), are relatively small. They consist primarily of the [2, 1] contribution; the [2, 2] contribution being essentially zero. For the initial [2, 1] contribution, roughly the center half of the bar width is in tension (compression), while the outside quarter-widths of the bar are in compression (tension), as indicated in Fig. 9(b) of Part 1. The effects do not entirely cancel and thus give rise to the small [2, 1] contribution. For the

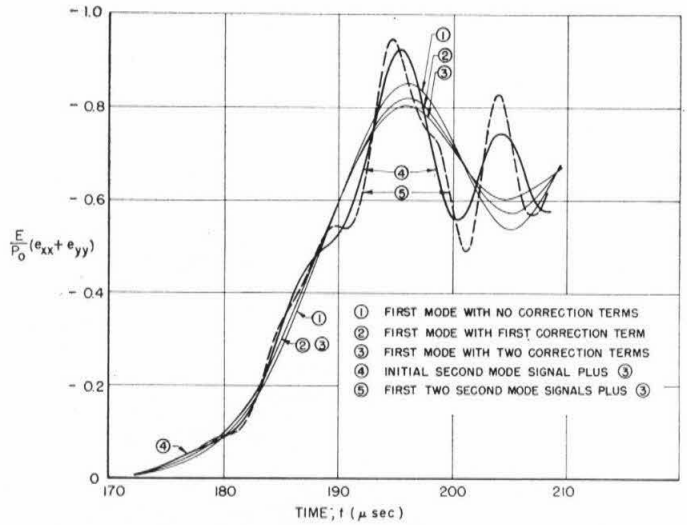

(a) $x = 37.5$ in.

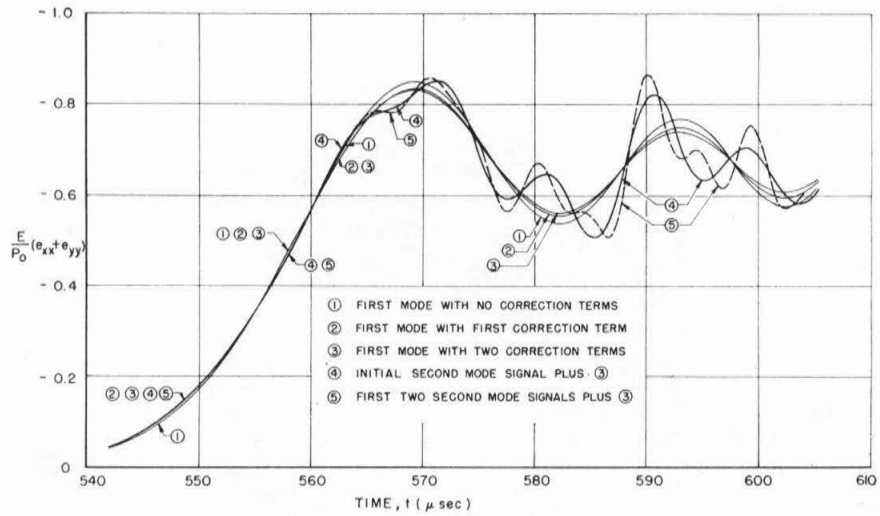

(b) $x = 112.5$ in.

Fig. 9 Predicted principal-strain sum $E(e_{xx} + e_{yy})/P_0$ at $y = 0$ for head of pulse. $c_s = 0.1248$ in. per microsec, $\sigma = 0.335$, $a = 0.75$ in.

initial [2, 2] contribution, roughly the portion of the bar width from $y = -a/4$ to $y = +a/4$ is in tension (compression), the portions from $y = a/4$ to $3a/4$ and from $y = -a/4$ to $-3a/4$ are in compression (tension), and the remaining portions are in tension (compression). The effects cancel almost exactly so that the initial [2, 2] contribution is negligible. Although the condenser-microphone records show some evidence of thickness-mode activity at the head of the pulse, the records for $x = 37.5$ and 112.5 in. are qualitatively very similar to the theoretical predictions.

Measured values for the dominant period $\bar{\tau}$ of the observed oscillations as a function of time are compared with predictions of the ordinary saddle-point analysis in Fig. 8 for the two stations. The experimental points appearing on these figures were determined from measurements made on the magnified records of Fig. 4. The half-period was measured from a peak (dip) to a dip (peak), and the full period was then assumed to occur at the mean of the time determining the half-period.

In agreement with the predictions discussed in the foregoing, the condenser-microphone measurements are clearly associated with the first mode. A trend seems to be present, however, indicating that the observed periods of the leading low-frequency oscillations become increasingly larger than the predicted periods as the distance of travel increases.

To study this possibility, the arrival times of the first peak and the intervals between the first peak and the first dip were measured carefully. The results of these measurements, along with the estimated limits of error, are compared in Tables 1 and 2 with the predicted first-mode values.

From Tables 1 and 2 it is apparent that the observed arrival times of the first peak and the time intervals between the first peak and the first dip are definitely larger than those predicted by the plane-stress theory and that the difference increases with increasing distance of travel. The implication, then, is that the low-frequency, long-wavelength components of the pulse are traveling at a lower velocity than predicted by the theory. This is in general agreement with the theoretical results of Gazis and Mindlin (see Part 1, reference [6]). Gazis and Mindlin studied the higher-order approximate Kane-Mindlin equations of motion which take into account the first symmetric extensional mode across the thickness. They showed that this thickness mode causes the low-frequency long-wavelength velocities of the first mode to be decreased from their corresponding plane-stress values. Also, they showed that the effect is accentuated for larger ratios of thickness to width. The observed values given in Table 2 appear to confirm this observation.

Detailed comparisons show that there is essentially no quantitative agreement between the predicted and observed amplitude

Table 1 Predicted and measured arrival times for first peak in condenser-microphone records

Station x, in.	Predicted first-mode arrival time, microsec		Measured arrival times, microsec Bar thickness, in.		
	Two terms	Three terms	0.064	0.126	0.252
37.5	195.82	196.34	197.9 ± 2.0	198.6 ± 2.0	197.5 ± 2.5
75.0	382.80	383.46	387.9 ± 2.1	387.2 ± 2.1	386.9 ± 2.6
112.5	568.87	569.62	583.1 ± 2.2	580.6 ± 2.2	579.3 ± 2.7

Table 2 Predicted and measured time intervals between first peak and first dip in condenser-microphone records

Station x, in.	Predicted first-mode time interval, microsec		Measured arrival times, microsec Bar thickness, in.		
	Two terms	Three terms	0.064	0.126	0.252
75.0	11.763	11.110	14.2 ± 1.0	15.2 ± 1.0	15.0 ± 1.0
112.5	13.466	12.718	15.4 ± 1.0	16.4 ± 1.0	16.9 ± 1.0

ratios of the first dip to the first peak. The poor reproducibility of the experimental records was reflected in a lack of any systematic order to the observed values. Since at least three records were obtained at each station for each bar, it should be pointed out that the spread in the amplitude ratios did not include the predicted values.

Comparison of Strain-Gage Records With Theory. The predicted barium-titanate, strain-gage response, which is proportional to the sum of the principal strains $(e_{xx} + e_{yy})$ at the center line $y = 0$ of the strip, is shown in Figs. 9(a) and (b) for the head of the pulse at stations $x = 37.5$ and 112.5 in., respectively. The first-mode contribution is obtained by evaluating (38) and (39) of Part 1 for $y = 0$ and summing the resulting expressions. The initial second-mode contributions are obtained by summing (45) and (46) of Part 1 and evaluating the resulting expression separately for each of the two initial second-mode arrivals. Similarly, second-mode contributions following the initial arrivals are obtained by summing and evaluating (48) and (49) of Part 1.

Figs. 9(a) and (b) show that the first-mode correction terms reduce the magnitude of the oscillations; however, their overall effect is much less important than it was for the predicted condenser-microphone response. The second-mode oscillations are actually present at a given station x for times preceding the arrival times given in Figs. 5 and 6. These oscillations, which have an approximately exponentially decreasing amplitude, are predicted by the extended saddle-point analysis.

Comparing the predicted strain-gage records of Figs. 9(a) and (b) with the corresponding experimental records in Fig. 4, it is evident, at least for the 0.252 and 0.126-in-thick bars, that the gross features of the observed behavior at the head of the pulse are qualitatively described by the theory if the [2, 2] contributions of the second mode are not considered. For example, considering the 0.252-in-thick bar record in Fig. 4 for station $x = 37.5$ in., it is seen that as time increases the amplitude gradually increases, undergoes a fairly abrupt increase in slope, continues to increase, levels off in a brief plateau, increases rapidly to a fairly sharp peak, falls off rapidly to a dip, and then rises sharply again. Without the [2, 2] contribution, the predicted record shown in Fig. 9(a) by the heavy solid line qualitatively exhibits all of these features. Except for thickness-mode effects, the gross behavior for the 0.126 and 0.064-in-thick bars is generally similar. In the same manner, a comparison of Figs. 4 and 9(b) for station $x = 112.5$ in. shows that the theory qualitatively exhibits the gross features of the observed records. It is interesting to note that the qualitative agreement is best at both stations for the 0.252-in-thick bar.

Retaining the [2, 2] contribution gives oscillations in the predicted strain-gage records which do not appear to have counterparts in the experimental records. Rejecting this contribution is not particularly disturbing since it strongly violates the assumptions on which the plane-stress approximation is based.

Conclusions and Remarks

Theoretical predictions based on the approximate plane-stress expressions developed in Part 1 for the propagation of a longitudinal elastic-strain pulse in a wide rectangular bar have been compared in detail with experimental observations. Fringe curvatures resulting from the warping of plane sections, as observed in pictures obtained using birefringent coatings and in the dynamic photoelastic pictures of other investigators, are qualitatively explained on the basis of this theory.

To provide more critical tests of the theory, an extensive experimental investigation using conventional measuring techniques was undertaken in which wide rectangular aluminum bars of several thicknesses were subjected to a pressure step produced by a shock tube. A condenser-microphone pickup was used to record changes in the width of the bars, and barium-titanate strain gages were used to record the sum of the principal strains midway between the edges of the bars. It has been shown that the gross features of the experimental records obtained with these detectors are qualitatively predicted on the basis of the plane-stress theory.

For reasonable distances of travel it has been shown that the plane-stress theory predicts that second-mode disturbances, which are generally not negligible, arrive shortly after the first-mode disturbance. This type of activity is strongly exhibited in the strain-gage records. Furthermore, the theory predicts that the short wavelengths associated with these second-mode disturbances violate the assumptions under which the plane-stress approximation should represent the actual bar behavior. Supporting this conclusion, the strain-gage records exhibit oscillations at the head of the pulse which are definitely associated with the bar thickness.

Careful studies of the condenser-microphone records reveal that low-frequency components of the first-mode oscillations travel at lower velocities than predicted by the plane-stress theory. Also, the velocities appear to be lower for larger ratios of bar thickness to width. It has been pointed out that these observations are in qualitative agreement with the theoretical results of Gazis and Mindlin (see Part 1, reference [6]) which were derived from the higher-order Kane-Mindlin approximate equations of motion which take into account the first symmetric thickness-stretch mode across the thickness.[8]

Quantitative comparisons of measured relative amplitudes from the experimental records do not agree with predicted plane-stress values. Even for the condenser-microphone records,

[8] It should be noted that the Kane-Mindlin equations of motion (see Part 1, reference [5]) are appropriate for including thickness effects only for small values of Poisson's ratio, inasmuch as, for $\sigma > 1/3$, there is at least one symmetric thickness-shear mode whose frequency is less than that of the lowest thickness-stretch mode. If effects due to symmetric thickness-shear modes are to be included, the approximate second-order equations of motion developed by Mindlin and Medick [10] must be used.

which are expected to be dominated by the first mode, the theory does not predict the observed values.

In general, then, the plane-stress theory appears to do a remarkably good job of predicting the qualitative behavior of the head of a strain pulse in a wide rectangular bar. However, it fails when quantitative tests are attempted. There are several possible reasons for this:

(*a*) Thickness modes may cause the true lowest mode solution to be sufficiently shifted from the corresponding approximate plane-stress solution so that quantitative values differ substantially while general qualitative agreement is still good. This was the situation in the case of the arrival time differences.

(*b*) For moderate distances of travel the early arrivals of higher-width modes, which have relatively high frequencies, may cause the different lateral end conditions between the theoretical and experimental problems to become important for the head of the pulse.

(*c*) An interesting observation should be made. The equations of motion for the symmetric vibrations of an infinite elastic plane-stress strip and for the corresponding vibrations of a cylindrical bar exhibit a very strong mathematical similarity (cf. Holden [11]). For the cylindrical bar they are the exact equations of motion. In contrast to the results discussed in the foregoing for wide rectangular bars, both theory and experimental results for cylindrical bars (see Part 1, references [9] and [10]) indicate that for moderate distances of travel the higher-mode contributions are either negligible or arrive late enough so that the first mode of the exact theory is adequate for quantitatively describing the head of the pulse. Also, it was pointed out in Part 1 that all of the important transient solutions for the step loading of a circular bar are either implicity or explicity based on the assumption that there is no warping of plane sections during the passage of the strain pulse. For cylindrical bars subjected to longitudinal step-pressure loading, Miklowitz and Nisewanger [12] are the only investigators who have made experimental measurements which might exhibit large effects due to nonuniform strain distributions across the diameter of the bar. Since they used a condenser microphone to measure changes in the bar diameter, the mathematical similarity just noted suggests that their experimental records for large distances of travel might exhibit warping contributions similar to those shown by the correction-term curves in Figs. 7 and 8. Miklowitz [7] observed just such discrepancies between his experimental results and theories based on plane sections remaining plane.

Thus, by retaining the correction terms in a similar manner as for the related plane-stress problem, it is possible to describe quantitatively effects resulting from the warping of plane sections in a cylindrical bar subjected to a step loading. The results of this analysis will be reported in the near future.

References

1 M. Hetényi, "Photoelasticity and Photoplasticity," *Structural Mechanics, Proceedings of the First Symposium on Naval Structural Mechanics*, Pergamon Press, New York, N. Y., 1960, pp. 483–505.

2 A. T. Ellis, "Techniques for Pressure Pulse Measurements and High-Speed Photography in Ultrasonic Cavitation," *Cavitation in Hydrodynamics*, Philosophical Library, Inc., New York, N. Y., 1957.

3 G. W. Sutton, "A Study of the Application of Photoelasticity to the Investigation of Stress Waves," PhD Thesis, California Institute of Technology, Pasadena, Calif., 1955.

4 J. C. Feder, R. A. Gibbons, J. T. Gilbert, and E. L. Offenbacher, "The Study of the Propagation of Stress Waves by Photoelasticity," *Proceedings of the Society for Experimental Stress Analysis*, vol. 14, 1956, pp. 109–117.

5 J. W. Dally, W. F. Riley, and A. J. Durelli, "A Photoelastic Approach to Transient Stress Problems Employing Low-Modulus Materials," JOURNAL OF APPLIED MECHANICS, vol. 26, TRANS. ASME, vol. 81, Series E, 1959, pp. 613–620.

6 A. J. Durelli and W. F. Riley, "Research Studies of Stress Waves in Earth and Model Earth Media," AFSWC Technical Report 60-4, Contract AF 29(601)1167, Project 1080, Task 10801, Armour Research Foundation, October, 1959, pp. 96–116.

7 J. Miklowitz, "On the Use of Approximate Theories of an Elastic Rod in Problems of Longitudinal Impact," *Proceedings, Third U. S. National Congress of Applied Mechanics*, ASME, New York, N. Y., 1958, pp. 215–224.

8 D. S. Hughes, W. L. Pondrom, and R. L. Mims, "Transmission of Elastic Pulses in Metal Rods," *Physical Review*, vol. 75, 1949, pp. 1552–1556.

9 J. W. Mark and W. Goldsmith, "Barium Titanate Strain Gages," *Proceedings of the Society for Experimental Stress Analysis*, vol. 13, 1955, pp. 139–150.

10 R. D. Mindlin and M. A. Medick, "Extensional Vibrations of Elastic Plates," JOURNAL OF APPLIED MECHANICS, vol. 26, TRANS. ASME, vol. 81, Series E, 1959, pp. 561–569.

11 A. N. Holden, "Longitudinal Modes of Elastic Waves in Isotropic Cylinders and Slabs," *Bell System Technical Journal*, vol. 30, 1951, pp. 956–969.

12 J. Miklowitz and C. R. Nisewanger, "The Propagation of Compressional Waves in a Dispersive Elastic Rod. Part II—Experimental Results and Comparison With Theory," JOURNAL OF APPLIED MECHANICS, vol. 24, TRANS. ASME, vol. 79, 1957, pp. 240–244.

Printed in U. S. A.